INSIDE VOLCANIC CLOUDS

Remote Sensing of Ash Plumes Using Microwave Weather Radars

BY FRANK S. MARZANO, ERRICO PICCIOTTI, MARIO MONTOPOLI, AND GIANFRANCO VULPIANI

Ash clouds due to volcanic eruptions can be detected in near–real time, quantitatively retrieved, and microphysically characterized by using ground-based microwave weather radars and their high-resolution spatial–temporal coverage.

Volcanic explosive eruptions probably represent one of the most devastating natural events for the surrounding environment, endangering people's lives and property (Wilson 1976; Barberi et al. 1990). The fragmentation of magma and parts of the volcanic system, through which the magma passes, generates particles that are collectively known as pyroclasts or tephra. Together with volcanic gases and entrained atmospheric air, they form the major constituents of a volcanic plume (Sparks et al. 1997; Prata et al. 1991). During a Plinian eruption, the injection of large amounts of fine and coarse rock fragments and corrosive gases into the troposphere and lower stratosphere is usually followed by a long-lasting ashfall (Wilson 1972; Valentine and Wohletz 1989; Clarke et al. 2002; Graf et al. 1999). Explosive volcanic eruptions can significantly influence climate, as well as cloud formation and global circulation, through atmospheric transport (Hood 1987; Armienti et al. 1988; Gobbi et al. 1992). Volcanic ash clouds are also an increasing hazard to aviation safety because of growing airline traffic (Casadevall 1994; Rose et al. 1995a; Tupper et al. 2007). From the first rudimental visual inspections at the times of Pliny the Elder, human curiosity and its need to find effective countermeasures to these extreme volcanic episodes has never ceased, even though their (fortunate) rarity makes scientific research quite challenging and, at the same time, the lives of people less anxious.

Microphysical characterization of Plinian volcanic ash plumes is usually carried out by analyzing tephra deposits and ash sedimentation on the ground

AFFILIATIONS: MARZANO—Department of Information Engineering, Electronics, and Telecommunications, Sapienza University of Rome, Rome, and Center of Excellence on Telesensing of the Environment and Model-Based Prediction Systems, University of L'Aquila, L'Aquila, Italy; PICCIOTTI—Center for Excellence on Telesensing of the Environment and Model-Based Prediction Systems, University of L'Aquila, and HIMET, L'Aquila, Italy; MONTOPOLI—Department of Geography, University of Cambridge, Cambridge, United Kingdom, and Center of Excellence on Telesensing of the Environment and Model-Based Prediction Systems, University of L'Aquila, L'Aquila, Italy; VULPIANI—Presidency of the Council of Ministers, Department of Civil Protection, Rome, Italy
CORRESPONDING AUTHOR: Dr. Frank S. Marzano, DIET, Sapienza University of Rome, Via Eudossiana 18, 00184 Rome, Italy
E-mail: marzano@die.uniroma1.it

The abstract for this article can be found in this issue, following the table of contents.
DOI:10.1175/BAMS-D-11-00160.1

In final form 25 February 2013

(Bonadonna and Phillips 2003; Koyaguchi and Ohno 2001). This analysis may only give indirect information on the ash cloud composition, as several processes can take place during the ash fallout (Clarke et al. 2002; Graf et al. 1999). On the other hand, real-time and spatial monitoring of a volcano eruption is not always possible by conventional visual analyses because of the usual low optical visibility (Riehle et al. 1994). Airborne flights within ash plumes using sample probes, as done for water clouds, are also considered too dangerous for the safety reasons previously mentioned (Casadevall 1994).

Remote sensing techniques represent a unique supporting tool to be exploited for this scope (Wen and Rose 1994; Krotkov et al. 1999). They allow for observation of the evolution of some key parameters of volcanic eruptions without direct interaction between the measurement system and the target of the measure. Electromagnetic or acoustic waves are usually employed to this aim. Until now, among the available remote sensing techniques, satellite-based approaches, using multifrequency radiometers with visible and infrared channels, have been demonstrated to be valuable support to the monitoring of ash clouds (e.g., Zehner 2010). However, they may suffer from poor spatial resolution if geosynchronous orbits (GEOs) are chosen and/or low revisiting time of the scene if low-earth orbits (LEOs) are used. Moreover, measurements in the visible spectral window are not available at night because of its solar illumination dependence, and the optical thickness of water and volcanic clouds can severely impair the sounding of lower cloud layers using ultraviolet up to infrared wavelengths (Rose et al. 2000; Vogfjörd et al. 2005; Prata et al. 2001). To circumvent the latter limitation, LEO-based microwave and millimeter-wave radiometers have been recently investigated for near-source ash plume detection and estimation (Marzano et al. 2013; Montopoli et al. 2013).

In contrast with satellite methodologies, ground-based microwave scanning weather radars can gather three-dimensional information of ash cloud scattering volumes with ranges up to some hundreds of kilometers in all weather conditions, at a fairly high spatial resolution (hundreds of meters) and with a repetition cycle of several minutes (Harris and Rose 1983; Rose et al. 1995a). In spite of this, the use of microwave radar for eruption monitoring has been very limited so far. Indeed, few theoretical and experimental research has been dedicated to this technique in the last decades (Harris and Rose 1983; Rose et al. 1995b; Maki et al. 2001; Lacasse et al. 2004; Marzano et al. 2006b; Donnadieu 2012). This is largely related to the predominant use of weather radars for meteorological operational forecasts and to the small number of volcanic areas that can be monitored by previously installed systems (Rose et al. 1995b; Marzano et al. 2006b). Plinian eruptions are indeed quite rare, in the sense that it is not frequent to observe a sustained eruption column (for many minutes to hours) fed directly from a substantial reservoir of magma. Much more common are Vulcanian explosions, which can also reach the stratosphere in many cases, but the jet phase may only last

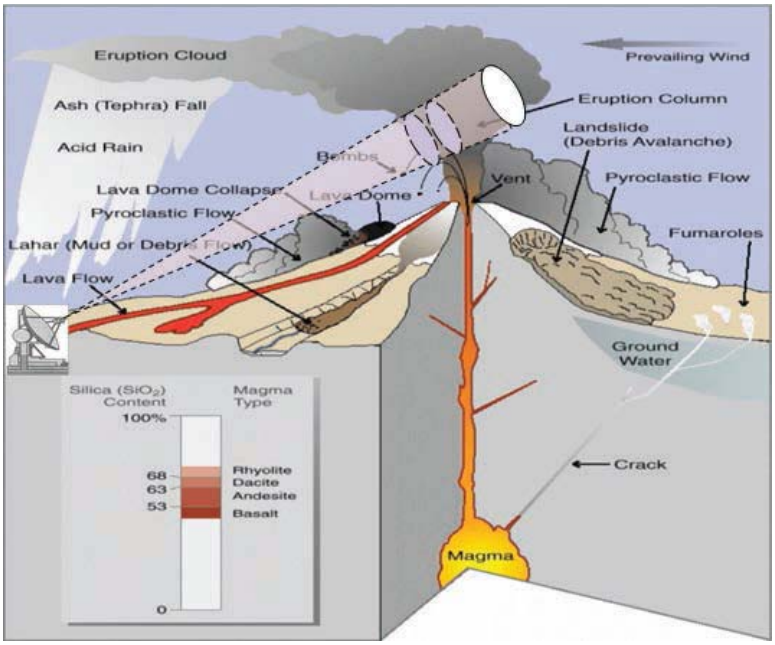

Fig. 1. Weather radar observation of an explosive volcanic eruption. Volcanic features are schematically indicated, as well as radar antenna beamwidth and range volume bin. The radar bin volume is determined by the range resolution (proportional to the pulse duration) and the transverse section of the radar antenna beamwidth. Note that the radar bin volume quadratically increases with the range. Thus, radars positioned at longer distances with respect to the volcano vent have reduced spatial resolution performances. Basic volcanological terminology is also introduced in terms of magma chamber and crack, volcano vent, eruption column and cloud (plume), lava flaw and dome, pyroclastic flow, tephra (ash, bomb), lahar, fumaroles, and landslide, considering a prevailing wind and magma type.

for several minutes and do not tap a deep reservoir directly. Retrieval techniques based on weather radar have much to tell us about Vulcanian explosions.

This paper illustrates and reviews the radar-based remote sensing of explosive volcanic eruptions, showing that a quantitative estimate of ash category and concentration can be nowadays accomplished with a fairly good degree of confidence within the radar coverage area. Several case studies of volcanic eruptions all over the world are described in order to demonstrate the potential of the radar retrievals of volcanic ash. Several examples of weather radar signatures at different frequency bands and radar-derived ash products are illustrated and discussed.

VOLCANIC ASH ERUPTIONS. The volcanic eruption is a geological phenomenon that involves the buoyant rise of magma from the deep layers of the Earth through fissures in the crust and onto the surface and throws up fragmented magma, as schematically depicted in Fig. 1. Materials of all types and sizes, erupting from a crater or volcanic vent as a result of an intensive magma and rock fragmentation, are usually referred to as *tephra*. The latter is mainly characterized by clast size, shape, and vesicularity, and ash is that component of tephra lower than 0.5 mm in diameter. Explosive eruptions occur when gases dissolved in molten rock (magma) expand and escape violently into the air, fragmenting the magmatic liquid.

Tephra can be ejected at speeds of several hundred meters per second and can rise rapidly to heights of several kilometers. The solid or liquid material in an eruption column is lifted by processes that vary as the material ascends. The region at the base of the column, where the pressure of expanding gases (mainly steam) forces the erupted material upward, is called the *gas thrust region,* which may extend up to a few kilometers. Under unstable conditions of the atmosphere into which the eruption column propagates, the ejected material is then lifted by convection. Most eruption plumes are dominantly convective. As the column rises upward, its density decreases and when it equals the density of the surrounding air, the eruption column stalls. The residual upward momentum, which the column still has from the convection region, allows the plume to rise a bit more and spread sideways, forming the so-called umbrella region. However, wind can quickly carry the plume away from the volcano and, because of the small vertical forcing in this region, the eruption column tends to spread horizontally (similarly to the anvil in the dissipation stage of a storm). As the cloud drifts downwind from the erupting volcano, coarser ash-falls from the cloud and the residual plume becomes finer grained.

The diameters of particles in fall deposits typically range from a few microns or less to several centimeters or more. Both the concentration and diameter of particles in the volcanic clouds decrease with distance from the vent because larger particles tend to fall out more near the vent. Table 1 summarizes the typical diameters, residence periods in the atmosphere, and the distance from the vent that volcanic debris can reach (Sparks et al. 1997). Major volcanic ash hazards—from air traffic impacts to mud flows, health risks, and climatic effects—are described in "Volcanic ash hazards."

VOLCANIC ASH RADAR MODELS. The observation geometry of radar remote sensing of explosive volcanic eruptions is schematically shown in Fig. 1. The radar bin volume ΔV is determined by the range resolution Δr (proportional to the duration of the pulse transmitted into the atmosphere), and the transverse section of the radar antenna beamwidth Θ_{3dB}. Note that radars positioned at longer distances with respect to the volcano vent have coarser spatial resolution and, as a consequence, reduced performances (see "Radar measurements of ash plumes" for an overview of weather radar basic concepts).

A physically based remote sensing technique needs a detailed physical–electromagnetic model to describe the interactions between microwaves and

Table 1. Main characteristics of volcanic pyroclasts (adapted from Rose et al. 2000 and Marzano et al. 2012b).

Tephra	Particle type	Typical particle size	Distance from the volcano vent	Residence time in the atmosphere
Ash	FA	<64 μm	Hundreds to thousands of kilometers	Days to months or years
	CA	64–532 μm	Tens to hundreds of kilometers	Days
Lapilli	SL	0.532–2.56 mm	Few to tens of kilometers	Few minutes
	LL	2.56–32 mm	Hundreds of meters to a few kilometers	Seconds to minutes
Blocks	BB	>32 mm	Tens to hundreds of meters	Tens of seconds

ash particles within each radar bin volume. To this aim we can exploit both experimental and modeling results to characterize ash particles (Bonadonna and Phillips 2003; Koyaguchi and Ohno 2001; Wohletz et al. 1989; Herzog et al. 1998; Veitch and Woods 2001; Textor et al. 2005). As shown in Table 1, most observations tend to classify volcanic cloud particles as ash, lapilli, and blocks [blocks and bombs (BB). The shape of tephra fragments can be complex, but it is usually approximated as equivalent spheres to simplify microphysical modeling and radiation calculations (Marzano et al. 2006b; Textor et al. 2005). Their composition and density are also quite variable depending on the type of eruption, possible aggregation processes, and environmental conditions (Valentine and Wohletz, 1989; Graf et al. 1999; Clarke et al. 2002; Donnadieu 2012). The distribution of ash-sphere-equivalent diameters has received a lot of attention and is generally deduced from sedimentation samples (Wohletz et al. 1989).

Ash particle occurrence per unit volume and unit size can be described by the particle size distribution (PSD) function whose general scaled form may be either a gamma or a Weibull function (Marzano et al. 2006b, 2010a):

$$N_p(D) = N_n \left(\frac{D}{D_n}\right)^{\mu} e^{-\Lambda_n \left(\frac{D}{D_n}\right)^{\nu}}, \qquad (1)$$

where D is the equivolume–spherical particle diameter (usually in mm), D_n is the number-weighted mean diameter, N_n is the PSD "intercept" (usually in $mm^{-1} \cdot m^{-3}$) for radar applications, Λ_n is the PSD "slope," μ is the PSD "shape" factor, and ν is the slope factor. The PSD normalization is such that N_n and Λ_n are related to mean diameter D_n, ash concentration C_a, and ash density ρ_a. The scaled-Weibull PSD can be derived from the segmentation–fragmentation–transport theory (Wohletz et al. 1989). The maximum-likelihood best fitting of Eq. (1) for available

VOLCANIC ASH HAZARDS

The explosive eruptions of active volcanoes with consequent formation of ash clouds represent a severe threat in several regions of the urbanized world (Prata et al. 1991). The injection of large amounts of fine and coarse ash and rock fragments and corrosive gases into the troposphere and lower stratosphere is usually followed by a long-lasting ashfall that can cause a variety of damages. Given the significance of the hazards posed by volcanic ash, timely detection and tracking of the erupted ash cloud is essential to a successful warning process, particularly during and immediately following an eruptive event (Tupper et al. 2007).

The ash ejected into the atmosphere by the Eyjafjöll Icelandic volcano during its recent eruption in 2010 posed such a threat to flights over much of Europe that the ensuing cancellations resulted in an unprecedented disruption of the international commercial air transportation system (Zehner2010). Volcanic ash represents a dramatic hazard for modern aircrafts (Casadevall 1994; Rose et al. 1995a). Eruptive ash is composed of silicates (above all aluminum and magnesium) and, once they are sucked up by jet engines of modern airplanes, they melt within the combustion chamber in which temperatures are almost equal to 1400°C. After crossing the combustion chamber, fused ashes solidify on turbine blades because of the lower temperature, reducing the engine performances up to complete failure. Since the ash is hard and abrasive, it corrodes the vehicle structure, flying areas, and engine components. Moreover, it causes abrasion and frosting of cockpit glass, and can cause the blockage of velocity and altitude controls up to their inefficiency. In addition, because of extremely small dimensions, volcanic ash is not stopped by common filtering systems, and can contaminate in a considerable way the air-conditioning systems as well as electric and flying ones enough to make the airplane hard to control.

Volcanic ash is not only a significant hazard to aircraft operations but also to public safety from volcanic ashfall at the surface. When volcanic ash accumulates on buildings, its weight can cause roofs to collapse. Because wet ash conducts electricity, it can cause short circuits and the failure of electronic components, especially high-voltage circuits and transformers. Eruption clouds and ashfall commonly interrupt or prevent telephone and radio communications in several ways, including physical damage to equipment and frequent lightning because of electrically charged ash particles. In the presence of subglacial volcanoes (as in Iceland), eruptions can cause a tremendous glacial burst flood (called jökulhlaup in Iceland). Fine ash may also be a health hazard, as aerodynamically fine particles will be taken into the lungs during breathing and may contaminate water resources.

Finally, volcanic ash is often accompanied by a very corrosive aerosol of sulphuric acid (H_2SO4), which is the result of the oxidation and hydration of sulphur dioxide (SO_2) released during the eruption phenomenon. This aspect is particularly dangerous for climate variations, since sulfate aerosols put into the stratosphere (10–50 km) can have a residence time of years because of the absence of precipitation at those altitudes. Thus, the portion of solar radiation reflected outward from the Earth increases with the resulting cooling of the upper stratosphere. On the other hand, even though the lower stratosphere appears to be cooling by about 0.5°C $decade^{-1}$, this cooling trend is interrupted by large volcanic eruptions that lead to a temporary warming of the stratosphere and may last for 1–2 years (Graf et al. 2007).

PSD ash measurements has indicated that the most probable value of μ is about 1 and 0.5, respectively, for a scaled-gamma and scaled-Weibull PSD (Marzano et al. 2006b).

The weather radar backscattered power is proportional to the "true" copolar horizontally polarized reflectivity factor Z_{hh}. Microwave scattering from ash particles and from cloud water and ice droplets typically satisfies the Rayleigh approximation for frequencies up to X band (about 3-cm wavelength) at least for fine and coarse ash (Marzano et al. 2010b). Under this condition, the simulated radar reflectivity factor Z_{hh} [conventionally expressed in $mm^6 \cdot m^{-3}$ or in corresponding decibels of reflectivity (dBZ)] due to an ensemble of particles p is expressed as the sixth moment of the PSD N_p following Sauvageot (1992):

$$Z_{hh} = \int_0^\infty D^6 N_p(D)\, dD. \qquad (2)$$

Thus, keeping constant the ash particle amount, the reflectivity factor is higher for bigger particles. Moreover, the variability of ash PSD modulates the radar reflectivity response.

Polarimetric Doppler radars can also measure the dual-polarization backscatter in both amplitude and phase (Bringi and Chandrasekar 2001). Vertically copolarized reflectivity Z_{vv} can be extracted as well as the horizontal one, Z_{hh}. The differential reflectivity Z_{dr} is defined as the ratio of reflectivity at the two orthogonal (horizontal and vertical) copolarization states (i.e., $Z_{dr} = Z_{hh}/Z_{vv}$), whereas the linear depolarization L_{dr} is the ratio between the cross polar (i.e., Z_{hv}) and the copolar reflectivity (i.e., $L_{dr} = Z_{hv}/Z_{hh}$). The copolar correlation coefficient r_{hv} (adimensional) is defined as the correlation between the radar echoes at horizontal and vertical polarization. Another important polarimetric parameter is the specific differential phase shift K_{dp} (° km^{-1}), which is due to the forward propagation phase difference between the two polarizations and can be estimated from the range derivative of the differential phase shift Φ_{dp} (i.e., $0.5 \times \Delta\Phi_{dp}/\Delta r$).

The interpretation and evaluation of the geophysical information content of polarimetric radar observables is not an easy task, especially if limited to the few available experimental analyses. From the available ash measurements on the ground, a microphysical model of volcanic clouds for radar observation purposes can be defined in terms of five main classes (or modes) of ash size: fine ash, coarse ash, small lapilli, large lapilli, and blocks (see Table 1). To simulate a wide variety of observation conditions, within each class, a random distribution can be assumed for, including i) average particle diameters (e.g., equal to 0.01, 0.1, 1, and 10 mm for fine, coarse, lapilli, and blocks, respectively); ii) average C_a with a mean value equal to 0.1, 1, and 5 g m^{-3} for light, moderate, and intense concentration regimes, respectively; and iii) angular average orientation labeled as prolate (when the particle major axis, assumed to have a spheroidal shape, is vertical with respect to the surface), oblate (when the predominant major axis is horizontal), and tumbling (when there is not any predominant orientation).

The correlation graphs among the radar polarimetric observables are sometimes called "self-consistency" plots. Indeed, this analysis is aimed at i) identifying the ash classes that can be actually discriminated with the available measurements and ii) evaluating the cross correlation and the possible cross domain of definition among the radar observables in order to perform a powerful quality check of the measurements once acquired and processed by the radar system. As an example, Fig. 2 illustrates a numerical simulation of the polarimetric radar signature at X band (Marzano et al. 2012b). The analysis of the results in Fig. 2 suggests that the copolar reflectivity depends on small, medium, and intense concentrations indicated with SC, MC, and IC, respectively. The differential reflectivity can distinguish among oblate (OO), prolate (PO), and tumbling (TO) orientation. The linear depolarization ratio may help to distinguish among oblate, prolate, and tumbling, whereas the signature of the correlation coefficient may help to discriminate among the PO, OO, and TO subclasses. The differential phase shift is sensitive to both medium and high concentrations. Moreover, the C_a and D_n are fairly well correlated with Z_{hh}. Previous considerations can be extended to S- and C-band weather radar observations as well. Thus, by fully exploiting the microphysical radar model and under its validity assumption, particle concentration, mean diameter, and fall rate (if the ashfall velocity is assumed) can be statistically derived from a combination of Z_{hh} and K_{dp}, whereas Z_{dr}, r_{hv}, and L_{dr} may be, in principle, used to better discriminate the ash classes.

Ash formation in the presence of free water can lead to a phreatomagmatic eruption. Phreatomagmatic is a term reserved for when magma effectively interacts explosively with liquid and/or ice water. It needs to be distinguished from particle and aerosol interactions with water vapor and/or ice (through condensation, nucleation, and aggregation processes) occurring once the plume has formed in the atmosphere. In such an eruption, two distinct particle combination

phenomena can occur within an observed range volume: i) coexistence of ash particle and hydrometeors and ii) aggregation (or mixture) of ash particles with hydrometeors to form a new mixed-phase particle. Numerical studies have showed that the particle combination processes, involving cloud liquid and frozen nonprecipitating particles within an ash plume, tend to reduce the radar reflectivity signature in a way dependent on the cloud particle distribution, ash mode, and aggregation process (Marzano et al. 2010a,b). For fine and coarse ash within a fractional combination with water particles of 50%, the expected reflectivity reduction is generally less than 1 dB for the coexistence process and less than 5 dB for the aggregation process with respect to the "dry" case (when neither coexistence or mixture processes happen).

VOLCANIC ASH RADAR OBSERVATIONS. A list of past weather radar measurements of volcanic plumes is provided in "Radar measurements of ash plumes." Most of these observations were only qualitatively reported and raw radar data were not available, unfortunately. Five recent volcanic eruptions, which will be analyzed in some detail later on, are selected in order to show the microwave radar capability to detected ash plumes and the potential of quantitative radar remote sensing of volcanic ash clouds. Different visual representations will be used to illustrate the richness of geophysical information carried out by a radar scan volume. Radar and volcano information, concerning the five examples mentioned above, are summarized in Table 2, and described briefly here.

1) Iceland is characterized by a significant subglacial volcanism that can have an influence on volcanic clouds (Wolfe et al. 1997; Gudmundsson et al. 1997; Björnsson 2002). Grímsvötn is one of the most active volcanoes in Iceland, with a caldera of about 62 km^2 covered by ice of thickness between 150 and 250 m (Sturkell et al. 2003). Its highest peak, Grímsfjall, on the southern caldera rim, reaches an elevation of 1722 m. The November 2004 eruption of the Grímsvötn volcano, located in the center of the 8100 km^2 Vatnajökull glacier, was a moderately sized eruption. The Keflavik weather radar is a C-band radar, located about 3 km north of the Keflavik International Airport at 47 m above sea level in southwestern Iceland and operated by the Icelandic Meteorological Office (IMO) (Lacasse et al. 2004). Its main operational characteristics are transmitted peak power P_t of 245 kW, antenna beamwidth of 0.9°, pulse duration τ of 2.15 μs, pulse repetition frequency of 250 Hz, and antenna gain of 44.9 dB. The C-band weather radar site is about 260 km west of the volcano, thus reducing the overall sensitivity to ash particles.

Data from the IMO Keflavik C-band radar every half hour have been made available by IMO from 2300 UTC 1 November 2004 to 0600 UTC 2 November 2004 every half hour. Reflectivity data, originally provided with a range resolution of 250 m, were smoothed to 2 km by a radial moving average. Figure 3 shows vertical cross sections [also

RADAR MEASUREMENTS OF ASH PLUMES

Weather radar systems, typically operated at S band (i.e., about 3 GHz or 10-cm wavelength), C band (i.e., about 5.6 GHz or 6-cm wavelength), and more recently X band (i.e., about 10 GHz or 3-cm wavelength), can be used to monitor and measure volcanic eruptions parameters although they are designed to study hydrometeors and rain clouds (Sauvageot 1992). Note that X-band radar, even though it was used for surveillance for many decades, was reconsidered for meteorological application only when the dual-polarized system was introduced as the measurement of the differential phase shift and can be used for two-way rain path attenuation correction. Both targets have the same measurement principle: both rain clouds and ash clouds feature fragmentation and aggregation processes and cause backscattering and absorption of the incident radiation, transmitted by radar (Bringi and Chandrasekar 2001).

Weather radars are usually pulsed Doppler monostatic (i.e., receiver and transmitter share the same antenna) systems with peak power between 10 kW and 1 MW, pulse duration between 0.1 and 2 μs, and a repetition period on the order of 1 μs. Range resolution is proportional to the pulse duration through the light velocity (and is on the order of tens of meters), whereas the nonambiguous maximum range r_{max} is related to the repetition period (and is up to several hundreds of kilometers). The ΔV is strongly limited by the transverse resolution, which is proportional to the antenna beamwidth Θ3dB and increases quadratically with respect to the range r (and this limits quantitative applications of weather radars to maximum ranges of a few hundred kilometers). Typical values for rmax, ΔV, Δr, and Θ3dB are 36–480 km, 6×10^4–6×10^8 m^3, 50–500 m, and 0.5°–3°, respectively. Typical Gaussian noise standard deviation of calibrated (zero bias) reflectivity measurements Z_{hhm} is on the order of 1 dBZ, whereas for polarimetric radar systems the uncertainty of Z_{drm}, K_{dpm}, ρ_{hv}, and L_{drm} is typically about 0.1 dB, 0.2° km^{-1}, 1%, and 1 dB, respectively, mostly dependent on data preprocessing and signal-to-noise ratio.

Table 2. Information about weather radar systems and volcanic eruptions of the five case studies described in the text.

Example	Event date	Volcano [elevation (m)]	Weather radar type and location [elevation (m)]	Distance between radar and volcano (km)
1	Nov 2004	Grímsvötn (1722)	Band C—single-polarization site; Keflavik (47)	265
2	Jan 2006	Augustine (1260)	Band S—single-polarization site; Kenai (50)	190
3	Apr–May 2010	Eyjafjöll (1666)	Band C—single-polarization site; Keflavik (47)	155
4	Apr 2011	Mount Etna (3350)	Band X—dual-polarization site; Catania (40)	30
5	May 2011	Grímsvötn (1722)	Band X—dual-polarization site; Vatnajokull (150)	70

The three-dimensional sampling of the atmosphere is obtained by azimuth and elevation rotation of the antenna (which is usually either a single or multireflector or a phased array). By exploiting the Doppler data processing, radial velocity v_r can be derived, whereas the recent capability of polarization diversity can provide an estimate of target asphericity, tumbling, and path attenuation. Cloud radars at Ka band (i.e., about 35 GHz or 0.8-mm wavelength) and at W band (i.e., about 90 GHz or 0.3-mm wavelength) are also now available. Note that the larger band is r_{max} and the lower band is the maximum detectable v_r due to the Doppler dilemma (Sauvageot 1992).

In 1970 the volcanic ash from the Hekla volcano was first observed in Iceland, while in the United States the first radar observations were performed during the eruption of the Augustine volcano in Alaska in 1976. During Mount St. Helens activity of 1980–82, there was the unique opportunity to collect observations using the U.S. National Weather Service radar system at C band in Portland, Oregon. These results were reported in detail by Harris and Rose (1983). There are other examples of volcanic ash detected by ground-based weather radar from 1970 to the present and the most important of them are listed in Table SB1.

Table SB1. Major explosive volcanic eruptions detected by ground-based weather radars from 1970 to 2011 (adapted from Sawada 2004 and Marzano et al. 2006b).

Year	Volcano	Location
1970	Hekla	Iceland
1973	Chaca	Kunashiri Islands, Japan
1976	Augustine	Alaska
1977	Usu	Hokkaido, Japan
1980	Mt. St. Helens	Washington
1981	Hekla	Iceland
1981	Pagan	Mariana Islands, Micronesia
1984	Sakurajima	Kyushu, Japan
1986	Izu Oshima	Izu Islands, Japan
1991	Pinatubo	Philippines
1991	Hekla	Iceland
1991	Unzen	Kyushu, Japan
1992	Spurr	Alaska
1992	Pinatubo	Philippines
1992	Unzen	Kyushu, Japan
1993	Unzen	Kyushu, Japan
1996	Sakurajima	Kyushu, Japan
1998	Popocatepetl	Mexico
1999	Popocatepetl	Mexico
2000	Miyake-jima	Izu Islands, Japan
2000	Hekla	Iceland
2000	Soufriere Hills	Montserrat, Caribbean
2002	Etna	Sicily, Italy
2004	Grímsvötn	Iceland
2006	Augustine	Alaska
2010	Eyjafjöll	Iceland
2011	Grímsvötn	Iceland
2011	Etna	Sicily, Italy

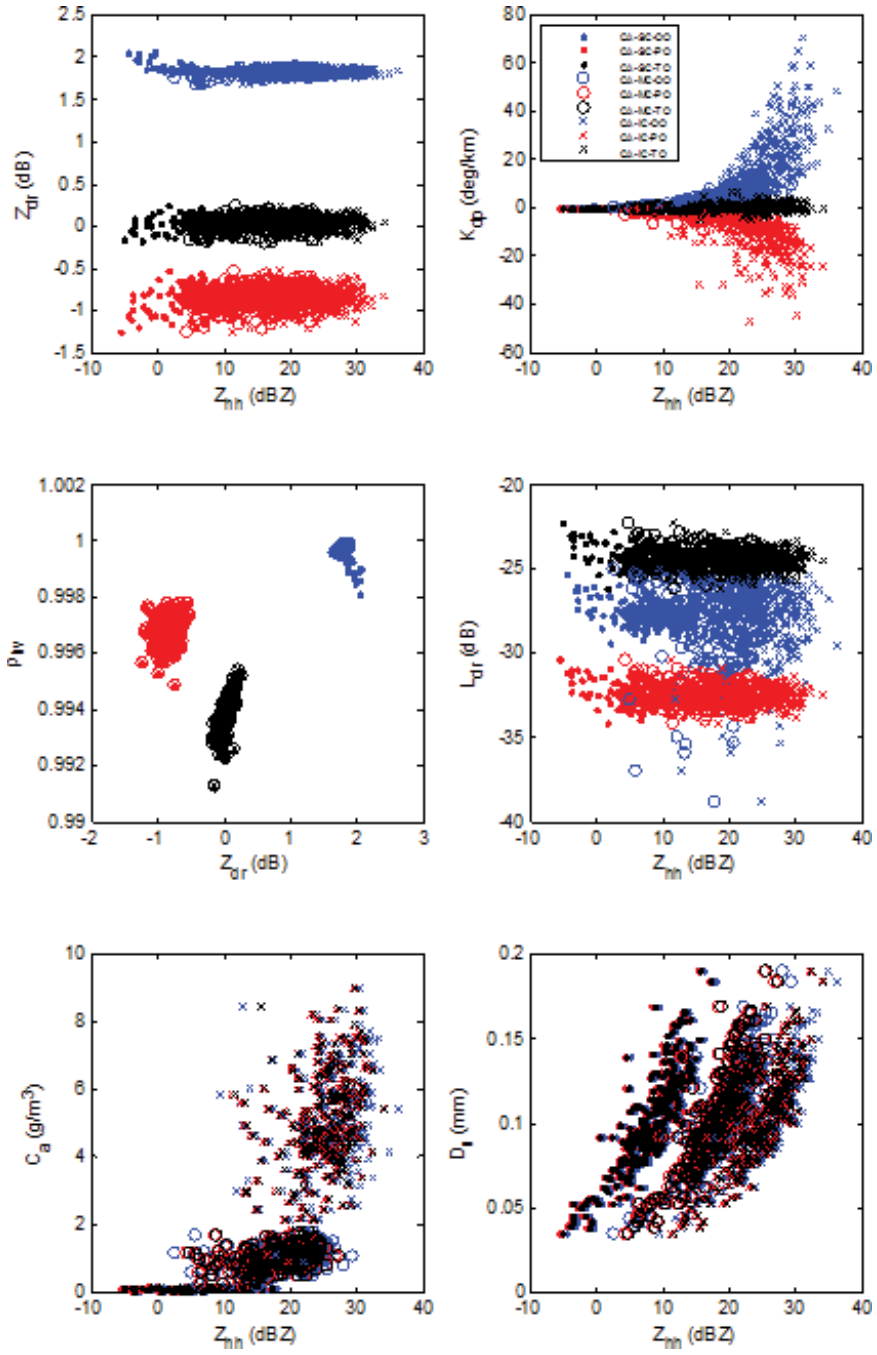

FIG. 2. (top and middle) Correlation between X-band polarimetric radar observables (Z_{hh}, Z_{dr}, K_{dp}, ρ_{hv}, L_{dr}) for CA size class, different volumetric concentration, and PO, OO, and TO, under the assumption of a basaltic–andesitic particle aspect ratio. (bottom) Correlation between ash concentration and mean diameter and Z_{hh}. Similar plots can be shown for FA and SL/LL and other frequency bands (C and S bands).

indicated by range–height indicators (RHIs) and obtained as a bidimensional cut of the available radar data volume] of the measured radar copolar reflectivity during the November 2004 eruption. The eruption plume, mainly coarse ash particles, reached a height of 6–10 km relative to the vent, as clearly detected by the C-band radar (Marzano 2011). Larger values of reflectivity are associated with bigger particles and/or higher particle concentration regions. This figure stresses the fact that the volcanic ash clouds can be detected from Keflavik only at heights higher than about 6 km using the minimum elevation of 0.5°. The signal of volcanic cloud is quite evident from the RHI signature with values up to 20 dBZ. At 0300 UTC the plume top altitude was about 15 km, even though this number may depend on the radar sensitivity (Marzano et al. 2010a).

2) The Augustine volcano is 1260 m high and is a conically shaped island stratovolcano located in the southern Cook Inlet, about 290 km (180 mi) southwest of Anchorage, Alaska. The Augustine volcano is the most active volcano in the Cook Inlet region. Figure 4 illustrates radar imagery interms of horizontal reflectivity maps [also called plan position indicators (PPIs), which are indeed ground projections of reflectivity conical volumes] for the Augustine volcano eruption in Alaska, which occurred around 1300 UTC 13 January 2006 and was observed by the S-band weather radar operated by the U.S. Geological Survey (USGS) Alaska Volcano Observatory (see Marzano et al. 2010b). In this case of an island volcano, radar remote sensing data represent very valuable information, since surface ash sampling

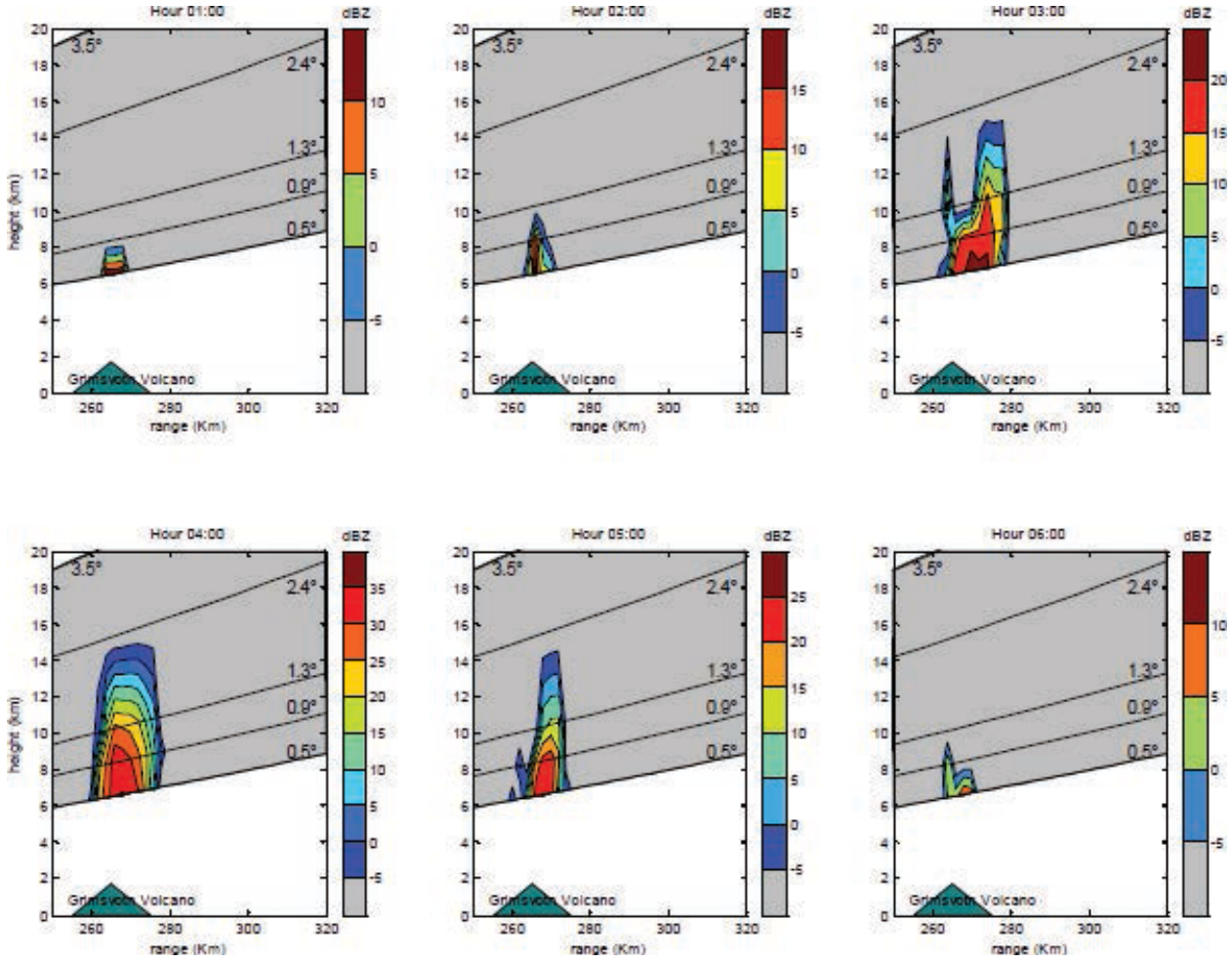

Fig. 3. C-band radar observations of the Grímsvötn eruption in 2004. RHI radar sections along the line of sight of about 265 km linking the C-band Keflavik radar and the vent of the subglacial Grímsvötn volcano at 0.5° elevation angle on 2 Nov 2004. (top) RHIs from 0100 to 0300 UTC. (bottom) RHIs from 0400 to 0600 UTC. The volcano vent is indicated by a triangle. Note that larger values of reflectivity are associated with bigger particles and/or higher particle concentration regions (adapted from Marzano et al. 2010a).

is almost impossible. The PPI image sequence clearly shows the spatial and temporal evolution of the ash plume.

3) The well-known Eyjafjöll eruption in 2010 was preceded by seismic activities around December 2009 that increased at the end of February 2010, leading to a small initial eruption (Gudmundsson et al. 2012). At 0600 UTC 14 April, the Eyjafjöll volcano resumed erupting after a small hiatus. The volcanic vent was under the glacier and the eruption became explosive and phreatomagmatic. On 15 April the ash cloud reached mainland northern Europe, thus forcing the closure of airspace (Zehner 2010). Figure 5 illustrates the Eyjafjöll volcano cloud in Iceland, observed between 14 and 19 April 2010 by the Icelandic Keflavik C-band weather radar (Marzano et al. 2011). Radar imagery is represented by very effective mixed horizontal–vertical maps [also denoted as horizontal–vertical maximum intensities (HVMIs)], such that on each subpanel the maximum reflectivity along a horizontal or vertical direction is shown. Note that the volcanic plume is concentrated near the volcano vent and that the other reflectivity signatures, closer to the radar, are due to ground clutter and possible precipitation cells. Ground clutter is usually removed, whereas meteorological targets are identified and properly labeled, after proper raw radar data processing.
4) The Mount Etna volcano is the major active European volcano, located in Sicily, Italy. A volcanic ash cloud, generated by the Etna eruption that occurred on 10 April 2011, was clearly

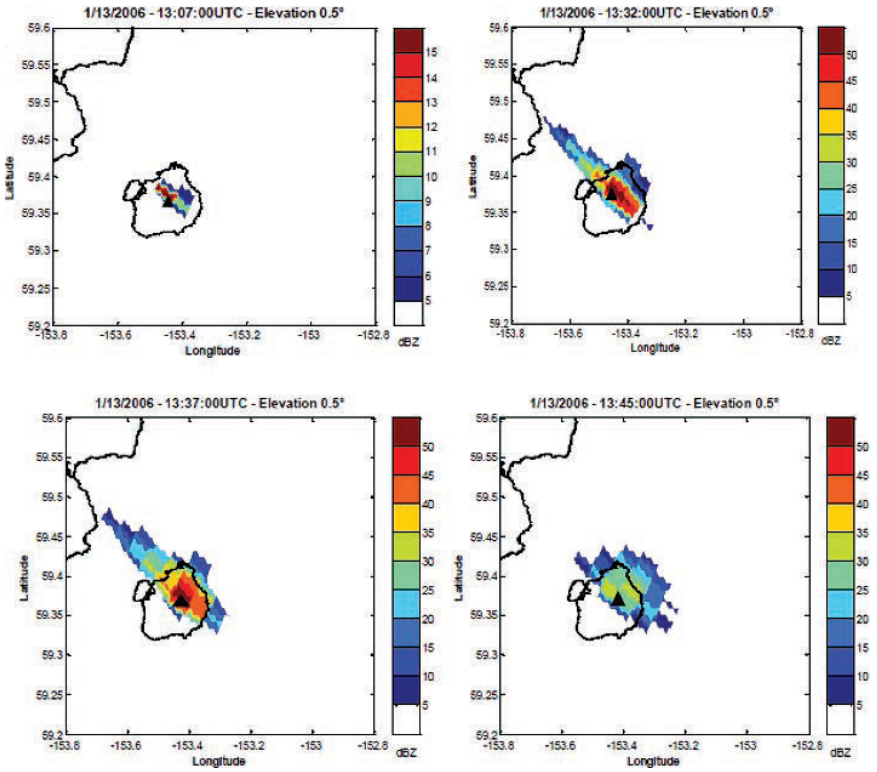

FIG. 4. S-band radar observations of Augustine volcanic eruption in 2006 (Alaska). PPI radar images of Augustine volcano eruption at 0.5° elevation of the S-band measured horizontally polarized reflectivity from 1307 to 1345 UTC 13 Jan 2006, the mature explosive phase of the eruption. Volcano vent is indicated by a black triangle. Radar data represent unique information—as in the case of Augustine island volcanoes, surface ash sampling is almost impossible. PPI image sequence clearly shows the spatial and temporal evolution of the ash plume (adapted from Marzano et al. 2010b).

observed by the mobile polarimetric X-band radar (named DPX4), located inside the Catania airport (about 30 km from from the volcano vent at 40 m above the sea level). The radar system, managed by the Italian Department of Civil Protection (DPC), is operationally used for either weather or volcanic ash monitoring, it being part of the national weather radar network (Vulpiani et al. 2005). Figure 6 shows RHI observations of the short ash eruption on 10 April 2011. The uniqueness of this dataset is that DPX4 is a dual-polarized X-band radar, so that we can have RHIs of ash cloud polarimetric signatures such as Z_{hh} (dBZ), Z_{dr} (dB), K_{dp} (° km^{-1}), and r_{hv} (adimensional) at a distance of about 70 km. As already mentioned, in the case of spherical ash particles, we would expect Z_{dr} to be equal to 1 (i.e., 0 dB), whereas we observe a pronounced spatial inhomogeneity especially in the ash layer closer to the ground.

5) The last example is a relatively recent Plinian eruption of the Grímsvötn volcano in Iceland, as previously mentioned. This eruption occurred in May 2011 and lasted for almost 10 days and was observed by an X-band polarimetric radar (named DPX1), identical to that used in Fig. 6. The DPX1 radar of DPC was deployed 70 km from the volcano vent and operated by IMO during the Grímsvötn volcanic activity. Figure 7 shows a HVMI image where the vertical sections are represented in a three-dimensional space this time (with respect to Fig. 5). As in Fig. 6, the relatively short range (70 vs 155 km in Fig. 5) enhances the spatial resolution and sensitivity of the radar to the ash plume. In the same figure lightning is also plotted, showing that lightning electrical activity may be intense, especially in the case of huge Plinian plumes that reached the height of 18 km. Fortunately, this plume moved northward, so that the European airspace was not affected.

VOLCANIC ASH RADAR RETRIEVALS. The retrieval of C_a and fall rate R_a from measured radar reflectivity Z_{hhm}, and, if available, from other polarimetric observables (such as Z_{drm}, K_{dpm}, r_{hv}, and L_{drm}), is a typical remote sensing inverse problem (Rogers 1976). Note that the subscript "m" indicates measured quantities (e.g., Z_{hhm}), which can differ from the true (modeled) ones without the same subscript (e.g., Z_{hh}) mainly because of system noise, residual clutter, and two-way path attenuation, as discussed later. As an inverse problem, it exhibits properties of nonuniqueness and instability of the solution. To circumvent this difficulty, the inverse problem can be stated as an estimation problem in a probabilistic framework (e.g., Rogers 1976; Marzano et al. 1999). A crucial role in this approach is played by the a priori information. This requires the construction of an effective

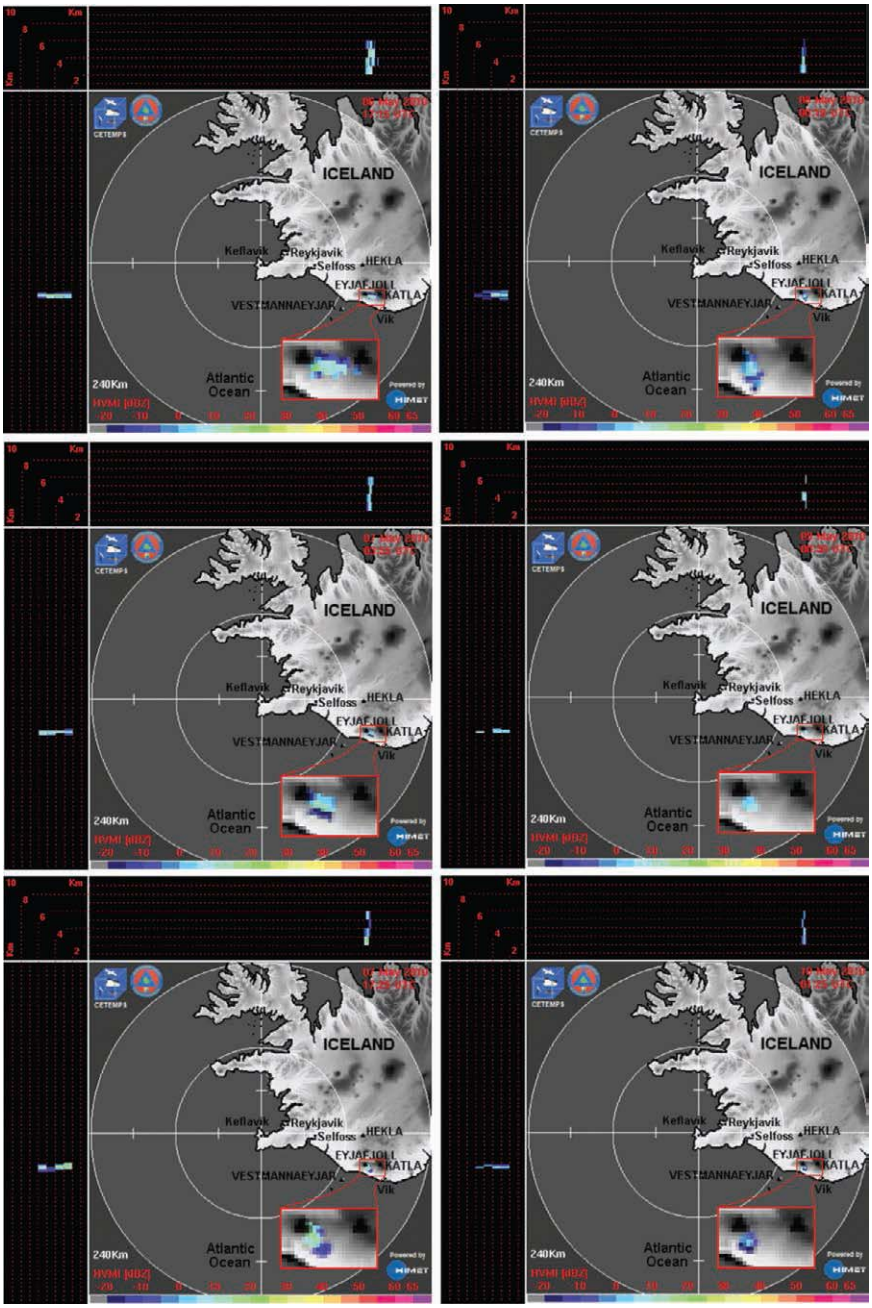

Fig. 5. C-band radar observations of the Eyjafjöll eruption in 2010 (Iceland). Six of the most significant HVMI radar images showing the recorded Keflavík C-band radar reflectivity (dBZ) from 1455 UTC 14 Apr to 2345 UTC Apr 19. Radar imagery is represented here by mixed HVMIs, such that in each panel the maximum reflectivity along a horizontal or vertical direction is shown. Each inset shows a zoom of the horizontal map close to the volcano vent. Note that the volcanic plume is concentrated near the volcano vent, whereas other reflectivity signatures due to ground clutter and possible precipitation cells have been filtered out through data processing (adapted from Marzano et al. 2011).

model able to describe the ash cloud microphysics and backscattering radar response.

The rationale of the volcanic ash radar retrieval (VARR) technique is summarized in Fig. 8. By exploiting the aforementioned microphysical ash model, a physically based volcanic ash radar retrieval algorithm can be designed as two successive steps:

i) detection of the ash class (see Table 1) from Z_{hhm} for single-polarization radars or a polarimetric observable set (i.e., in general, Z_{hhm}, Z_{drm}, K_{dpm}, r_{hv}, and L_{drm}) for dual-polarization radars within each range bin by using a Bayesian identification technique, and
ii) retrieval of C_a (g m^{-3}) and R_a (kg h^{-1} m^{-2}) from either the measured Z_{hhm} or polarimetric observable set by applying a nonlinear regression or iterative Bayesian optimal estimation methodology.

The Bayesian techniques may be thought as a generalization of fuzzy logic methods where the membership functions of each ash category, listed in Table 1, can be interpreted as probability density functions (e.g., Marzano et al. 2007, 2008). Among the Bayesian approaches, the maximum a posteriori probability (MAP) criterion can be used to carry out cloud classification in a model-based supervised context (e.g., Marzano et al. 1999, 2006a). The basic rule is to minimize a proper "distance" (metric) between the measured reflectivity Z_{hhm} (or measured polarimetric set) and the corresponding centroid in terms of true Z_{hh} (or polarimetric set), computed by using the microphysical scattering of each ash class, taking into account both the system noise and the a priori available information (see "Radar measurements of

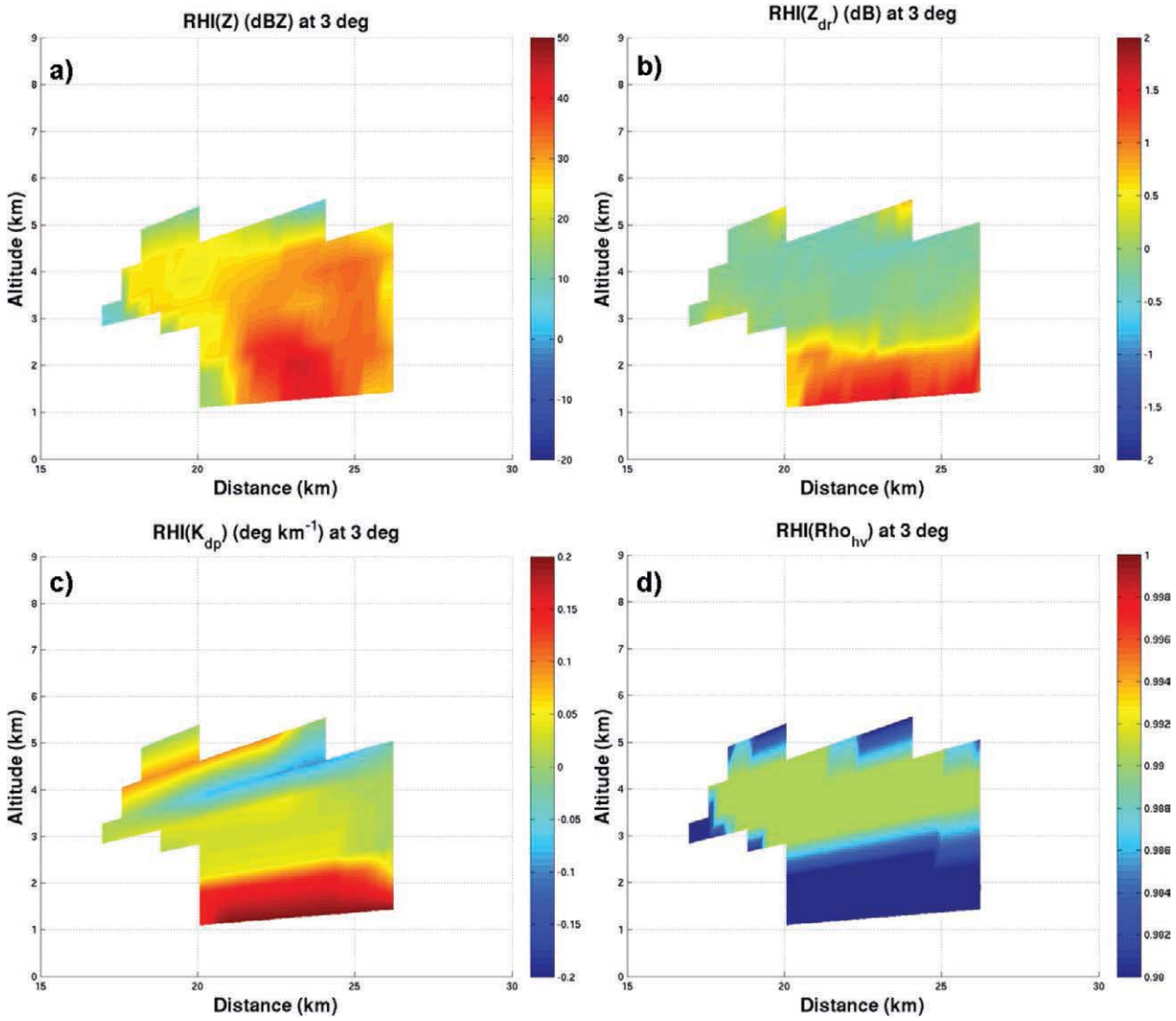

Fig. 6. X-band radar observation of the Mount Etna eruption in 2011 (Italy). RHIs at 3° of azimuth of (a) Z_{hh}, (b) Z_{dr}, (c) K_{dp}, and (d) ρ_{hv} as retrieved from a volumetric scan at 1330 UTC 10 Apr 2011 at a distance of about 70 km from the vent. Note that in case of aspherical ash particles Z_{dr} is different from 1 (or, equivalently in Decibel logarithmic units, different from 0 dBs), whereas a pronounced spatial inhomogeneity is observed in the ash layer closer to the ground.

ash plumes"). The estimated ash class is the one that exhibits the minimum Bayesian distance given the radar measurement set.

Once an ash class is detected, then an estimate of C_a and R_a is possible. A way to approach the quantitative retrieval problem is to adopt a forward model to describe the relation x–Y_m, where x stands for either C_a or R_a belonging to the identified class and Y_m is a polarimetric observable within the available set of radar measurements (see Fig. 2, where the nonlinear correlation between C_a and Z_{hh} can be clearly exploited). The VARR estimation algorithm can be formulated either iteratively or analytically if an analytical relation (e.g., power law or polynomial) between x and Y_m is assumed.

The microwave weather radar response is mainly controlled by the PSD of microphysical species within the range volume bin, as shown by Eq. (2). Several caveats need to be accepted to properly deal with radar products. The major critical issues are as follows: i) conical observation geometry inevitably produces occluded regions at longer ranges and in the presence of obstacles (e.g., a mountain or even the volcano vent); ii) the radar ash detectability depends not only on the receiver sensitivity but also quadratically on the inverse distance, so that only larger particles can leave a radar signature at longer ranges; iii) because of the centimeter wavelength of the radar signal, fine ash is hardly detected, so that most microwave radar

signatures detect the near-source plume, depending on the sedimentation and settling of coarse ash and lapilli (see Table 1)—indeed, fine ash represents only a small portion of total tephra and can be transported far from the volcano vent (Wen and Rose 1994); iv) the discrimination between ash and hydrometeors and the identification of ash–water aggregates is beyond the current capabilities of weather radar and should be treated as an ambiguity (uncertainty) affecting the qualitative and quantitative interpretation of the radar imagery of ash clouds; v) for ash monitoring below Ku band (12–18 GHz), the specific attenuation, due to fine and coarse particles and gas absorption along the beam, is usually lower than 1 dB km^{-1}, but it can increase greatly above the Ku band (Marzano et al. 2006b) as well as below the Ku band for high particle concentrations; vi) at longer ranges (longer than 120 km), the radar volume bin may have a transverse cross section larger than a few kilometers (the radial resolution is governed by the pulse width and can be as short as hundreds of meters), which may produce some ash content error because of the nonuniform antenna beam filling (Kitchen and Jackson 1993; Zrnić and Rhyzkov 1996); and vii) the system noise can degrade the quality of radar observables, and its level is discussed in "Radar measurements of ash plumes." The radar noise bias can be reduced by a proper systematic calibration, whereas its standard deviation can be smoothed by space–time averaging (Sauvageot 1992).

Some of the above-mentioned limitations may be overcome by using polarimetric measurements and using higher-frequency systems in order to increase the radar sensitivity to ash (Marzano et al. 2012b). But, even with dual-polarized Doppler radars, it is very difficult to discriminate between coexistence or aggregation of ash and hydrometeors by looking at their respective signatures (e.g., Marzano et al. 2012b; Marzano et al. 2007, 2008). Moreover, at higher frequencies the path attenuation can become a further problem with which to deal (Marzano et al. 2006b). Eventually, the performances of the polarimetric VARR algorithm will be affected by the accuracy and completeness of the polarimetric model of ash radar response.

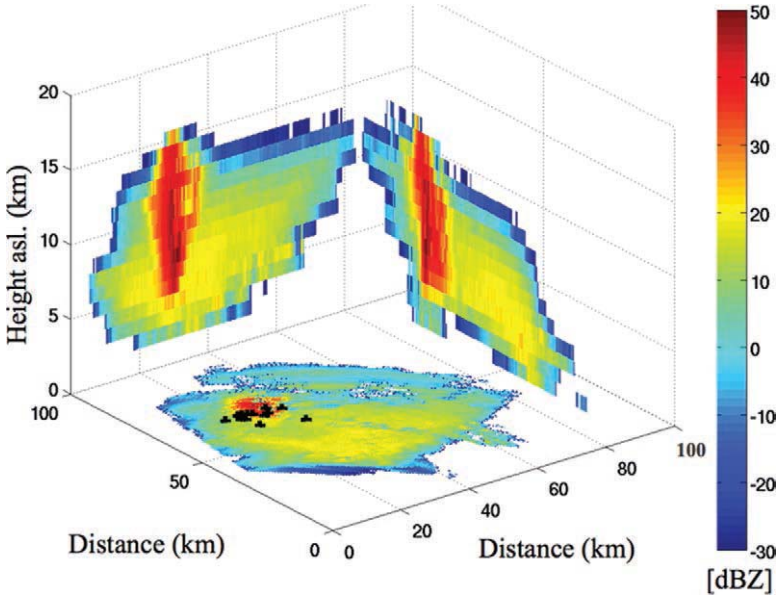

Fig. 7. X-band radar observation of the Grímsvötn volcanic eruption on 22 May 2011 (Iceland). HVMI Z_{hh} reflectivity (dBZ) image at 0612 UTC, where the maximum of radar reflectivity volume along the vertical and horizontal directions is considered around the volcano vent. The X-band radar, supposed to be in the position (0, 0), is located at about 70 km from the volcano. The 15 detected lightning positions, projected to the ground, are also plotted as black symbols, showing that lightning electrical activity may be intense for Plinian plumes.

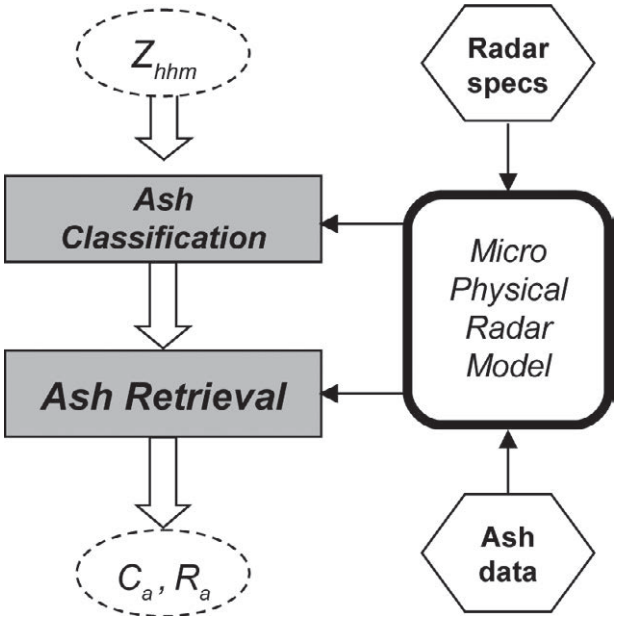

Fig. 8. Schematic block diagram of the VARR algorithm depicting the classification and the retrieval stages, trained by the microphysical radar model parameterized by radar specifications (specs) and ash available data. In the case of polarimetric radars (e.g., see Figs. 2, 6, and 7), inputs to VARR may include not only Z_{hhm} but also Z_{drm}, ρ_{hv}, K_{dpm}, and L_{drm}.

Many of the above-mentioned errors might be corrected with ancillary information (e.g., satellite data, lidars, ceilometers, and video camera systems) that is not always available with the same space–time resolution of ground radars. To deal with these uncertainties, we can estimate them in terms of error average and variance, and introduce this variability into the Bayesian retrieval algorithm. This is a conservative choice, as the ash estimate standard deviation will increase, but it is a rigorous way to introduce this lack of knowledge within the inversion algorithm. On the other hand, any advancement in the understanding of the observed ash clouds can be, in principle, incorporated within the forward model of the physically based VARR technique in order to improve its validity and reduce its uncertainty.

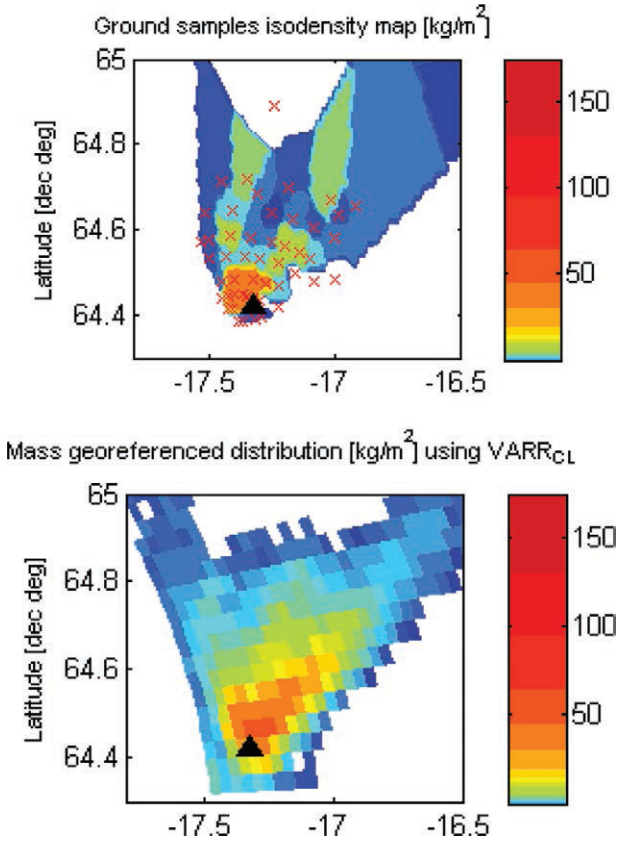

Fig. 9. Grímsvötn eruption in 2004. Maps of in situ–measured and radar-retrieved tephra loadings. (top) The 69 processed sample's positions superimposed on the interpolated isodensity map. (bottom) Results from the VARR$_{CL}$ algorithm (calibrated by using an ash mean density and diameter derived from collected thephra deposits, and by assuming a constant vertical profile of reflectivity from the minimum detectable height to the ground). Black triangle is centered in the exact position of the Grímsvötn volcano. Color bars are scaled to match the different dynamic ranges of the tephra loading distribution (adapted from Marzano et al. 2012a).

VOLCANIC ASH RADAR PRODUCTS. We now show some products of the VARR processing when observing a volcanic eruption. To appreciate the potential of these outputs, we should compare the radar-based ash morphological and physical estimates we can derive at such high space–time resolution with classical volcanological sampling that is usually carried out after the end of the eruption. Of course, the ground sampling remains essential for radar-based calibration, intercomparison, and validation; however, in a way radar and ground sampling can be seen as complementary, with the radar playing the role of space–time "extrapolator" of static a posteriori ground data.

Grímsvötn eruption in 2004. As shown in Fig. 3, the eruption started in Grímsvötn on the evening of 1 November 2004 and was detected by the C-band weather radar. The instantaneous volcanic ash cloud volume V_{aC} (m^3), which represents the detected volume of the ash cloud at a given nominal time step t, can be estimated by using a threshold on the estimated concentration C_a, the threshold being related to the minimum detectable reflectivity. However, as noted in Fig. 3, the total portion of V_{aC} is not detectable by the scanning radar, thus inducing an underestimate of the total ash volume and mass because of the radar observation geometry and the presence of partial obstructions along the ray paths. To partially overcome this problem, we can apply a simple reconstruction of the vertical profile of reflectivity (VPR), based on the assumption of a reflectivity constant value, down to the surface, equal to the lowest measured reflectivity (Marzano et al. 2011, 2012a). The drawback of this approach is a possible erroneous estimation of the ash mass should the concentration change with height and vice versa.

Using the time series of V_{aC}, the instantaneous airborne ash mass M_a (kg) can be estimated from each radar bin volume. The deposited ash at the ground (tephra loading) during the eruption event can be estimated from the retrieved R_a, estimated from radar measurements (see Marzano et al. 2012a for details). The interest in the retrieval of the tephra mass loading is that it can be directly compared with the ground sampling of ash. A variety of methods have been used to calculate deposit volumes (Bonadonna and Houghton 2005; Fierstein and Nathenson 1992; Pyle 1989; Rose et al. 1973). All of these methods are empirical and based on thickness measurements of tephra. In the case of the Grímsvötn eruption in 2004, ground mass loading or ash depth was directly derived from the weight of

the dried tephra in the snow cores obtained in situ in the 5–50-km range during the summers of 2005 and 2006 (Marzano et al. 2012a).

Deposited ash mass loadings, evaluated in terms of spatial maps (note that they are not "distal" in terms of fine ash transport), are shown in Fig. 9. The VARR-estimated spatial patterns compare fairly well with the ground-sampled mass loading used for validation, as shown in Fig. 9. The spatial collocation of radar-based estimates and ground measurement allows pixel-by-pixel comparison between the retrieved and the deposited ash mass. This comparison should be evaluated with some care, as it refers to a spatially integrated mapping from radar versus spatial interpolation of point measurements from ground sampling. Nevertheless, it is an appealing way to perform the cross validation in terms of not only total mass but also spatial distribution of the deposited ash. As expected, the correlation is not unitary because of ground data interpolation errors and radar retrieval algorithm inaccuracy and obstructed geometry observation. The correlation coefficient is about 0.55, whereas the root-mean-square error (RMSE) is about 27 kg m^{-2}. Total mass radar-based estimation provides a value between 0.36×10^{10} and 5.72×10^{10} kg, depending on the VARR data-processing technique, with a further 10% of variability because of the surface ash variability and an additional 30% because of the fallout velocity model. Ground-measured ash loading is about 5.60×10^{10} kg, which is in relatively good agreement with the estimated variability derived from radar-based retrievals (Marzano et al. 2012a). The results, considering all the unknowns involved, are very encouraging and may represent a first essential step for validating VARR retrievals on the ground.

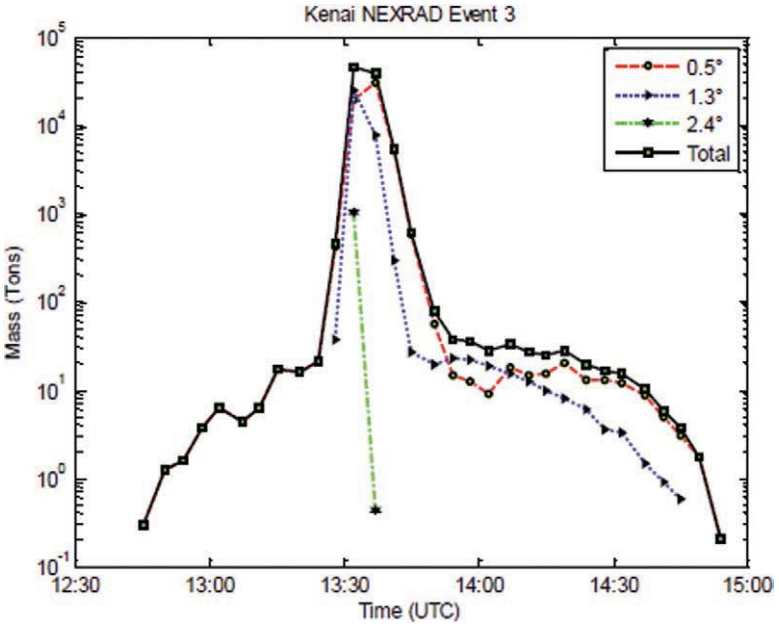

Fig. 10. Augustine eruption in 2006. PPI-referred mass content of eruptive material retrieved by the Kenai radar at 0.5°, 1.3°, and 2.4° elevations and total retrieved mass content (from all PPIs) with respect to the time, during the observation of explosive event 3 around 1300 UTC 13 Jan 2006. Total retrieved columnar content is given from the sum of the columnar contents estimated for the elevation scans at the three elevation angles and available from the Kenai radar (adapted from Marzano et al. 2010a).

Augustine eruption in 2006. In the case of the Augustine eruption during the winter season, it may happen that ash nucleates ice early in ash cloud history; indeed, during the eruption abundant water vapor was ejected and the temperature was well below the freezing point at the lower altitudes. We can expect that all observed ash was subject to ice accretion processes and we must assume, within the radar microphysical forward model, that ash clouds were composed of solid ash, hydrometeors, and ash aggregates that were made by a mixture of ash and ice (Marzano et al. 2010b).

Starting from the results from the VARR retrieval algorithm of the estimated mass particle concentration within the volcanic cloud at all times and at all elevations, and using the information about the scanning strategy employed during the third eruption observed, we have also estimated the radar-retrieved columnar content of eruptive material. Figure 10 shows the PPI-based mass content of the eruptive material retrieved by the Kenai radar at 0.5°, 1.3°, and 2.4° elevations and the total retrieved mass content considering all PPIs, with respect to time, during the observation of explosive event 3. The peak of the total retrieved columnar content at 1332 UTC corresponds to the Vulcanian explosive phase, when a larger amount of eruptive material is ejected. In this phase the estimated particle concentration within the ash cloud and consequently the total mass content assume their maximum values. Note that the scan geometry of the Kenai radar limits the mass integration to heights higher than 4 km at a range of 190 km around the Augustine volcano.

Eyjafjöll eruption in 2010. The $V_{aC}(t)$ (m^3), which represents the volume of the ash cloud at a given t (the latter is referred to as "instantaneous," even though the radar takes about two minutes to complete a volume scan), may be estimated by using a threshold on the estimated concentration $C_a(t)$ at a given position. The temporal trend of the instantaneous total mass $M_a(t)$, retrieved by VARR by integrating the estimated $C_a(t)$ over the cloud volume $V_{aC}(t)$, is shown in Fig. 11 using the available datasets. The instantaneous trends of $V_{aC}(t)$, obtained by multiplying $M_a(t)$ by a constant ash density r_a (in this case, equal to 1200 kg m^{-3}), are also shown in the same figure for the same time window. During the May episode, the most intense day was on 5 May with an instantaneous ash mass up to 8×10^7 kg. It is interesting to note i) the intermittent and pulsed temporal character of the Eyjafjöll eruption and ii) the long and gradual waning phase of the 5 May event, which lasted more than six days.

The spatial distribution of the instantaneous maximum plume height can be then derived by using a threshold on the retrieved C_a. The instantaneous maximum ash cloud height $H_{aM}(t)$, with respect to all ground coordinates, can be also computed at each instant t. The maximum plume height $H_{aM}(t)$ is an important input parameter in most volcanological models, forecasting the volcanic eruption intensity and the most useful quantity to aerial route planning in the areas near the volcanic eruption (Stohl et al. 2011). The plume height estimation shows some variability because of the altitude discrete sampling of radar beams at given elevations and radar beam

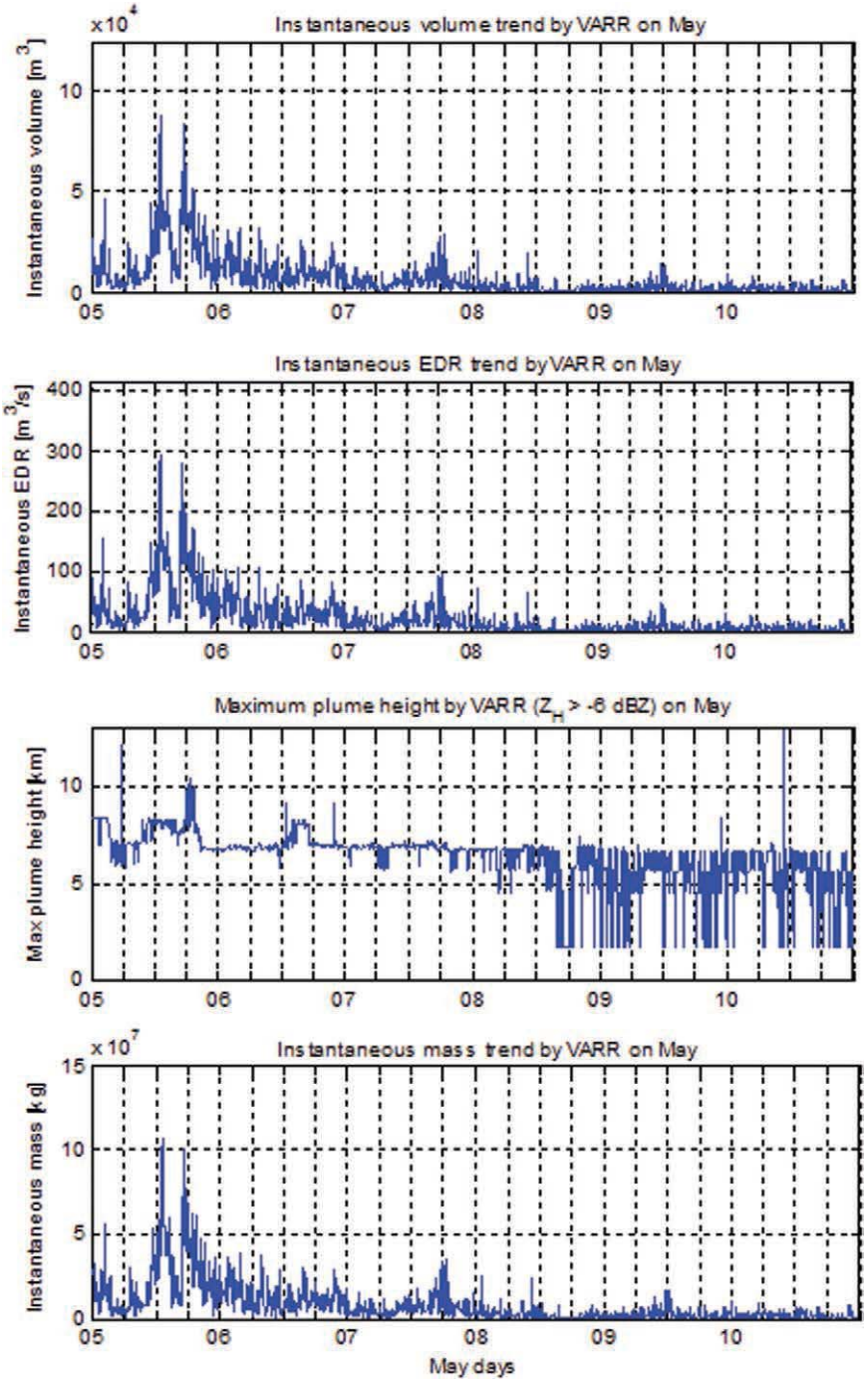

Fig. 11. Eyjafjöll eruption in 2010. Instantaneous volume, EDR, maximum plume height, and instantaneous mass (obtained from R_a estimated by VARR) vs time (scan days) with reference to the eruptions on the May time window (from 0010 UTC 5 May 2010 to 2355 UTC 10 May 2010). Ticks on the *x* axis have a spacing equal to 6 h. Scan sampling period is equal to 5 min, so that the time series shows a time window of about 8630 min (143.8 h) since the first available radar data at 0010 UTC 5 May 2010 with reference to the dataset of May (adapted from Marzano et al. 2011).

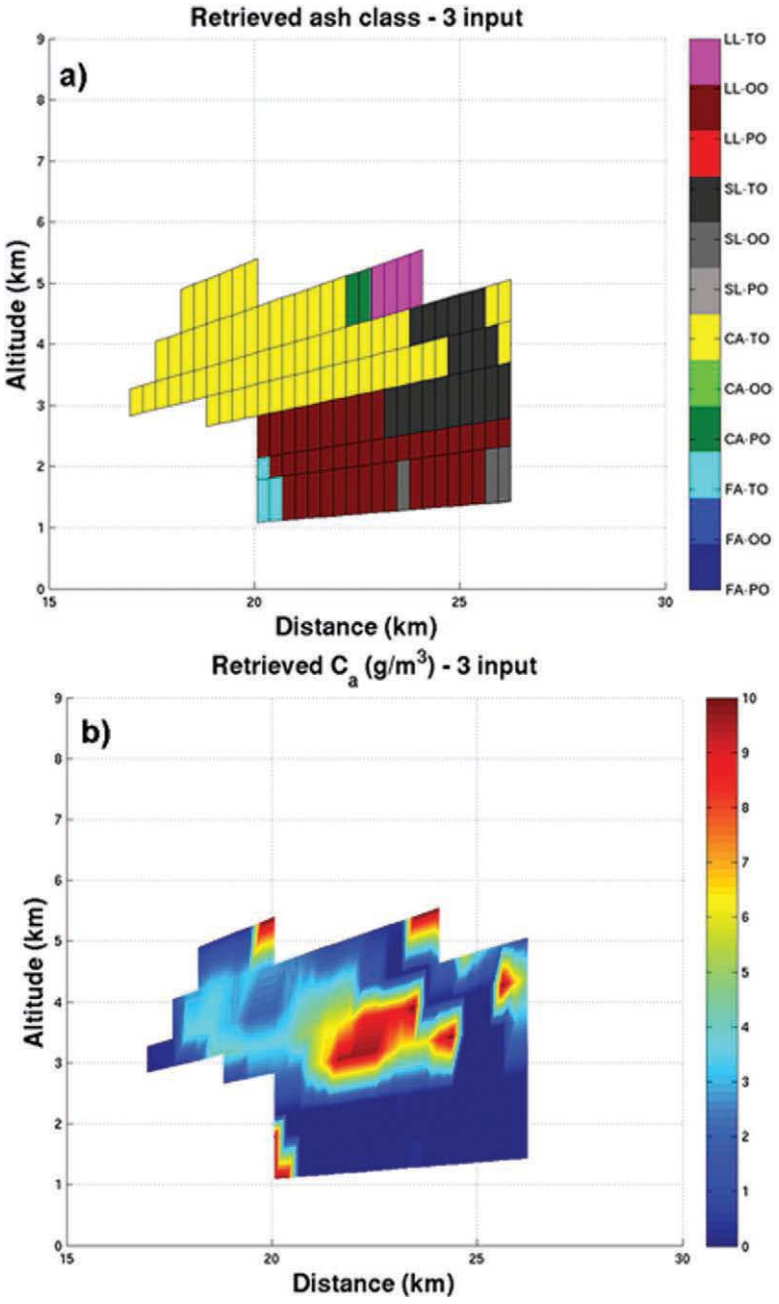

Fig. 12. Etna eruption in 2011. RHIs at 3° azimuth of the (a) estimated volcanic ash classes and (b) retrieved C_a, related to measurements shown in Fig. 6. Spatial distribution of ash classes resembles the evolution of the radar reflectivity. Prevailing identified ash class is LL with OO. At relatively high altitudes and distances farther than a few kilometers, FA and CA are more likely to be expected. Spatial pattern of estimated C_a does not strictly resemble that of radar reflectivity in Fig. 6 because a given reflectivity may be due to either a low concentration of bigger particles or a high concentration of smaller particles.

occlusions. The estimated maximum height is up to 10 km.

The maximum plume height retrievals H_{aM}, provided by weather radars, can be used to compute the eruption discharge rate (EDR), a useful parameter to mark the intensity of a volcanic eruption (Wilson 1972; Sparks et al. 1997). When the EDR is known, it is possible to estimate the thickness of the ash layer that will settle on the ground according to a model widely used for eruption columns that produce strong plumes (Wilson et al. 1978). Theoretical relations show that EDR is linked to the fourth power of the height and so small fluctuations of the height imply large variations of the EDR. Figure 11 also shows the estimated EDR for the May period. The estimate of EDR evidences that the May event shows peaks less than 300 $m^3 s^{-1}$, with more intense activity on 5 May 2010.

Etna eruption in 2011. The echoes, observed in Fig. 6 at altitudes higher than the Mount Etna volcano peak (about 3.2 km above sea level) at distances between 10 and 40 km (where lapilli are not expected because of their ballistic trajectories, which limit their fall to few kilometers from the vent), were found to be characterized by equivalent reflectivity factor values ranging between a few decibels to about 35 dBZ, while Z_{dr} was found to be symmetrically distributed between −0.5 and 0.5 dB. If the VARR classification algorithm is applied to radar RHI data, it is possible to detect the ash class, as shown in Fig. 12. The spatial distribution of ash classes in Fig. 12 resembles the evolution of the radar reflectivity. The prevailing identified ash class is the large lapilli (LL) with OO. At relatively high altitudes and distances farther than a few kilometers, the fine ash (FA) and coarse ash (CA) are more likely to be expected with respect to small lapilli (SL) and, especially, large LL. This might lead to inferences that the results obtained above 3000 m may be questionable even if its estimated pattern is not improbable, considering the Mount Etna peak is at 3350 m (from Fig. 12 we have SL near the vent and CA in the surrounding region).

Figure 12 also shows the results in terms of estimated C_a obtained by applying the VARR retrieval technique to the measured reflectivity RHI data (Marzano et al. 2012b). By applying the VARR classification, we can address this ambiguity by identifying the predominant ash particle category. This is particularly evident below 3000 m for all VARR input configurations, where the low amount of lapilli causing high radar reflectivity is contiguous to regions of large amounts of coarse ash particles.

CONCLUSIONS. The potential of using ground-based weather radar systems for volcanic ash cloud detection and quantitative retrieval has been widely illustrated and evaluated. Radar observations are mainly sensitive to coarse ash and lapilli because of typical receiver sensitivities, which, indeed, may depend on radial distances. A physical–statistical technique to estimate ash size, concentration, and fallout has been described, underlying its physical background and theoretical framework. The VARR inversion methodology has been quantitatively applied to recent eruptions in Iceland, Alaska, and Italy, discussing its main features in terms of achievable products. A quantitative validation of the radar-derived ash concentrations has been discussed for the Icelandic eruption in 2004 using subsurface drilling ash data. It is worth noting that what was remotely retrieved in the upper troposphere is not necessarily consistent with ground deposits collected after the eruption.

Indeed, the validation of radar-derived ash plume retrievals is a critical issue: with respect to rain clouds, the possibility to perform airborne campaigns through eruptive volcanic clouds is too unsafe for human pilots, as mentioned earlier. An appealing future might be the use of unmanned airborne vehicles (UAVs) with ad hoc jet engines so that solid particle spectrometers could be operated without human risk. A further validation might be carried out by using ground-based disdrometers, similar to those used for raindrop size distribution measurements, tuned for ash-particle detection.

The synergy between ground-based weather radars and other remote sensors and the exploitation of ash plume forecasting models is a major future goal, especially for what concerns the characterization of the near-source eruption environment. Scanning optical lidars may complement microwave radars for fine-ash-dispersed plume detection, whereas millimeter-wave radars may also be employed for increasing the detection capability. Satellite passive and active sensors, both GEO and LEO based, may significantly benefit the ash fallout and deposit estimate over large areas for retrieval intercomparison and experimental validation.

ACKNOWLEDGMENTS. This work was partially funded by the Italian Department of Civil Protection (Rome, Italy) under the stimulus of past vice head B. De Bernardinis and Sapienza University of Rome; the Marie Curie Fellowship within the call FP7-POPLE-2010-IEF, Grant 273666; and the FP7 project FUTUREVOLC "A European volcanological supersite in Iceland: A monitoring system and network for the future" (Grant Agreement 308377). We are grateful to P. Crochet (IMO, Iceland), R. Hannesen (SelexSI-Gematronik, Italy), and B. Palmason (IMO, Iceland) for providing radar data. The fruitful cooperation of S. Barbieri (DIET, Italy), G. Ferrauto (CETEMPS, Italy), and M. Lamantea (DIET, Italy) is deeply acknowledged.

REFERENCES

Armienti, P., G. Macedonio, and M. T. Pareschi, 1988: A numerical model for simulation of tephra transport and deposition: Applications to May 18, 1980, Mount St. Helens eruption. *J. Geophys. Res.,* **93** (B6), 6463–6476.

Barberi, F., G. Macedonio, M. Pareschi, and R. Santacroce, 1990: Mapping the tephra fallout risk: An example from Vesuvius, Italy. *Nature,* **344,** 142–144.

Björnsson, H., 2002: Subglacial lakes and jökulhlaups in Iceland. *Global Planet. Change,* **35,** 255–271.

Bonadonna, C., and J. C. Phillips, 2003: Sedimentation from strong volcanic plumes. *J. Geophys. Res.,* **108,** 2340, doi:10.1029/2002JB002034.

——, and B. F. Houghton, 2005: Total grain-size distribution and volume of tephra-fall deposits. *Bull. Volcanol.,* **67,** 441–456.

Bringi, V. N., and V. Chandrasekar, 2001: *Polarimetric Doppler Weather Radar: Principles and Applications.* Cambridge University Press, 636 pp.

Casadevall, T. J., Ed., 1994: Volcanic ash and aviation safety: Proceedings of the First International Symposium on Volcanic Ash and Aviation Safety. USGS Bull. 2047, 450–469.

Clarke, A. B., B. Voight, A. Neri, and G. Macedonio, 2002: Transient dynamics of vulcanian explosions and column collapse. *Nature,* **415,** 897–901.

Donnadieu, F., 2012: Volcanological applications of Doppler radars: A review and examples from a transportable pulse radar in L-band. *Doppler Radar Observations: Weather Radar, Wind Profiler, Ionospheric Radar, and Other Advanced Applications,* J. Bech and J. L. Chau, Eds., InTech, 409–446.

Fierstein, J., and M. Nathenson, 1992: Another look at the calculation of fallout tephra volumes. *Bull. Volcanol.,* **54,** 156–167.

Gobbi, G. P., F. Congeduti, and A. Adriani, 1992: Early stratospheric effects of the Pinatubo eruption. *Geophys. Res. Lett.,* **19,** 997–1000.

Graf, H. F., M. Herzog, J. M. Oberhuber, and C. Textor, 1999: The effect of environmental conditions on volcanic plume rise. *J. Geophys. Res.,* **104** (D20), 24 309–24 320.

——, Q. Li, and M. A. Giorgetta, 2007: Volcanic effects on climate: Revisiting the mechanisms. *Atmos. Chem. Phys.,* **7,** 4503–4511.

Gudmundsson, M. T., F. Sigmundsson, and H. Björnsson, 1997: Ice–volcano interaction of the 1996 Gjálp subglacial eruption, Vatnajökull, Iceland. *Nature,* **389,** 954–957.

——, and Coauthors, 2012: Ash generation and distribution from the April–May 2010 eruption of Eyjafjallajökull, Iceland. *Sci. Rep.,* **2,** 572, doi:10.1038/srep00572.

Harris, D. M., and W. I. Rose Jr., 1983: Estimating particle sizes, concentrations, and total mass of ash in volcanic clouds using weather radar. *J. Geophys. Res.,* **88** (C15), 10 969–10 983.

Herzog, M., H.-F. Graf, C. Textor, and J. M. Oberhuber, 1998: The effect of phase changes of water on the development of volcanic plumes. *J. Volcanol. Geotherm. Res.,* **87,** 55–74.

Hood, R. B., 1987: Numerical advection algorithms and their role in atmospheric transport and chemistry models. *Rev. Geophys.,* **25,** 71–100.

Kitchen, M., and P. M. Jackson, 1993: Weather radar performance at long range—Simulated and observed. *J. Appl. Meteor.,* **32,** 975–985.

Koyaguchi, T., and M. Ohno, 2001: Reconstruction of eruption column dynamics on the basis of grain size of tephra fall deposits: 1. Methods. *J. Geophys. Res.,* **106** (B4), 6499–6512.

Krotkov, N. A., D. E. Flittner, A. J. Krueger, A. Kostinski, C. Riley, W. Rose, and O. Torres, 1999: Effect of particle non-sphericity on satellite monitoring of drifting volcanic ash clouds. *J. Quant. Spectrosc. Radiat. Tranfer,* **63,** 613–630.

Lacasse, C., S. Karlsdóttir, G. Larsen, H. Soosalu, W. I. Rose, and G. G. J. Ernst, 2004: Weather radar observations of the Hekla 2000 eruption cloud, Iceland. *Bull. Volcanol.,* **66,** 457–473.

Maki, M., K. Iwanami, R. Misumi, R. J. Doviak, T. Wakayama, K. Hata, and S. Watanabe, 2001: Observation of volcanic ashes with a 3-cm polarimetric radar. *Proc. 30th Int. Conf. on Radar Meteor.,* Munich, Germany, Amer. Meteor. Soc., P5.13. [Available online at https://ams.confex.com/ams/30radar/techprogram/paper_21897.htm.]

Marzano, F. S., 2011: Remote sensing of volcanic ash cloud during explosive eruptions using ground-based weather radar data processing. *IEEE Signal Process. Mag.,* **28,** 124–126, doi:10.1109/MSP.2010.939846.

——, A. Mugnai, G. Panegrossi, N. Pierdicca, E. A. Smith, and J. Turk, 1999: Bayesian estimation of precipitating cloud parameters from combined measurements of spaceborne microwave radiometer and radar. *IEEE Trans. Geosci. Remote Sens.,* **37,** 596–613.

——, S. Barbieri, G. Vulpiani, and W. I. Rose, 2006a: Volcanic cloud retrieval by ground-based microwave weather radar. *IEEE Trans. Geosci. Remote Sens.,* **44,** 3235–3246.

——, G. Vulpiani, and W. I. Rose, 2006b: Microphysical characterization of microwave radar reflectivity due to volcanic ash clouds. *IEEE Trans. Geosci. Remote Sens.,* **44,** 313–327.

——, D. Scaranari, and G. Vulpiani, 2007: Supervised fuzzy-logic classification of hydrometeors using C-band weather radars. *IEEE Trans. Geosci. Remote Sens.,* **45,** 3784–3799.

——, ——, ——, and M. Montopoli, 2008: Supervised classification and estimation of hydrometeors using C-band dual-polarized radars: A Bayesian approach. *IEEE Trans. Geosci. Remote Sens.,* **46,** 85–98.

——, S. Barbieri, E. Picciotti, and S. Karlsdóttir, 2010a: Monitoring subglacial volcanic eruption using C-band radar imagery. *IEEE Trans. Geosci. Remote Sens.,* **58,** 403–414.

——, S. Marchiotto, C. Textor, and D. Schneider, 2010b: Model-based weather radar remote sensing of explosive volcanic ash eruption. *IEEE Trans. Geosci. Remote Sens.,* **48,** 3591–3607.

——, M. Lamantea, M. Montopoli, S. Di Fabio, and E. Picciotti, 2011: The Eyjafjöll explosive volcanic eruption from a microwave weather radar perspective. *Atmos. Chem. Phys.,* **11,** 9503–9518.

——, ——, ——, B. Oddsson, and M. T. Gudmundsson, 2012a: Validating subglacial volcanic eruption using ground-based C-band radar imagery. *IEEE Trans. Geosci. Remote Sens.,* **50,** 1266–1282.

——, E. Picciotti, G. Vulpiani, and M. Montopoli, 2012b: Synthetic signatures of volcanic ash cloud particles from X-band dual-polarization radar. *IEEE Trans. Geosci. Remote Sens.,* **50,** 193–211.

——, M. Lamantea, M. Montopoli, M. Herzog, H. Graf, and D. Cimini, 2013: Microwave remote sensing of the 2011 Plinian eruption of the Grímsvötn Icelandic volcano. *Remote Sens. Environ.,* **129,** 168–184.

Montopoli, M., D. Cimini, M. Lamantea, M. Herzog, H. Graf, and F. S. Marzano, 2013: Microwave radiometric

remote sensing of volcanic ash clouds from space: Model and data analysis. *IEEE Trans. Geosci. Remote Sens.,* **51,** in press, doi:10.1109/TGRS.2013.2260343.

Prata, A. J., I. J. Barton, R. W. Johnson, K. Kamo, and J. Kingwell, 1991: Hazard from volcanic ash. *Nature,* **354,** 25.

Prata, F., G. Bluth, W. Rose, D. Schneider, and A. Tupper, 2001: Comments on "Failures in detecting volcanic ash from a satellite-based technique." *Remote Sens. Environ.,* **78,** 341–346.

Pyle, D. M., 1989: The thickness, volume and grainsize of tephra fall deposits. *Bull. Volcanol.,* **51,** 1–15.

Riehle, J. R., W. I. Rose, D. J. Schneider, T. J. Casadevall, and J. S. Langford, 1994: Unmanned aerial sampling of a volcanic ash cloud. *Eos, Trans. Amer. Geophys. Union,* **75,** 137–138.

Rogers, C. D., 1976: Retrieval of atmospheric temperature and composition from remote measurement of thermal radiation. *Rev. Geophys.,* **14,** 609–624.

Rose, W. I., S. Bonis, R. E. Stobier, M. Keller, and T. Bickford, 1973: Studies of volcanic ash from two recent Central American eruptions. *Bull. Volcanol.,* **37,** 338–364.

——, and Coauthors, 1995a: Ice in the 1994 Rabaul eruption cloud: Implications for volcano hazard and atmospheric effects. *Nature,* **375,** 477–479.

——, A. B. Kostinski, and L. Kelley, 1995b: Real-time C band radar observations of 1992 eruption clouds from Crater Peak, Mount Spurr volcano, Alaska. The 1992 eruptions of Crater Peak vent, Mount Spurr volcano, Alaska, USGS Bull. 2139, 19–26.

——, G. J. S. Bluth, and G. G. J. Ernst, 2000: Integrating retrievals of volcanic cloud characteristics from satellite remote sensors: A summary. *Philos. Trans. Roy. Soc. London,* **A358,** 1538–1606.

Sauvageot, H., 1992: *Radar Meteorology.* Artech House, 366 pp.

Sawada, Y., 2004: Eruption cloud echo measured with C-band weather radar. [Available online at www.ofcm.noaa.gov/ICVAAS/Proceedings2004/pdf/entire-2ndICVAAS-Proceedings.pdf.]

Sparks, R. S. J., M. I. Bursik, S. N. Carey, J. S. Gilbert, L. Glaze, H. Sigurdsson, and W. Woods, 1997: *Volcanic Plumes.* Wiley and Sons, 574 pp.

Stohl, A., and Coauthors, 2011: Determination of time- and height-resolved volcanic ash emissions and their use for quantitative ash dispersion modeling: the 2010 Eyjafjallajökull eruption. *Atmos. Chem. Phys.,* **11,** 4333–4351, doi:10.5194/acp-11-4333-2011.

Sturkell, E., P. Einarsson, F. Sigmundsson, S. Hreinsdóttir, and H. Geirsson, 2003: Deformation of Grímsvötn volcano, Iceland: 1998 eruption and subsequent inflation. *Geophys. Res. Lett.,* **30,** 1182, doi:10.1029/2002GL016460.

Textor, C., H. F. Graf, M. Herzog, J. M. Oberhuber, W. I. Rose and G. G. J. Ernst, 2005: Volcanic particle aggregation in explosive eruption columns. Part I: Parameterization of the microphysics of hydrometeors and ash. *J. Volcanol. Geotherm. Res.,* **360,** 359–377.

Tupper, A., I. Itikarai, M. S. Richards, F. Prata, S. Carn, and D. Rosenfeld, 2007: Facing the challenges of the International Airways Volcano Watch: The 2004/05 eruptions of Manam, Papua New Guinea. *Wea. Forecasting,* **22,** 175–191.

Valentine, G. A., and K. H. Wohletz, 1989: Numerical models of Plinian eruption columns and pyroclastic flows. *J. Geophys. Res.,* **94** (B2), 1867–1887.

Veitch, G., and A. W. Woods, 2001: Particle aggregation in volcanic eruption columns. *J. Geophys. Res.,* **106** (B11), 26 425–26 441.

Vogfjörd, K. S., and Coauthors, 2005: Forecasting and monitoring of subglacial eruption in Iceland. *Eos, Trans. Amer. Geophys. Union,* **86**, 245–252, doi:10.1029/2005EO260001.

Vulpiani, G., F. S. Marzano, V. Chandrasekar, and S. Lim, 2005: Constrained iterative technique with embedded neural network for dual-polarization radar correction of rain path attenuation. *IEEE Trans. Geosci. Remote Sens.,* **43,** 2305–2314.

Wen, S., and W. I. Rose, 1994: Retrieval of sizes and total masses of particles in volcanic clouds using AVHRR bands 4 and 5. *J. Geophys. Res.,* **99** (D3), 5421–5431.

Wilson, L., 1972: Explosive volcanic eruptions – II. The atmospheric trajectories of pyroclasts. *Geophys. J. Roy. Astron. Soc.,* **30,** 381–192.

——, 1976: Explosive volcanic eruptions – III. Plinian eruption columns. *Geophys. J. Roy. Astron. Soc.,* **45,** 543–556.

Wilson, L., R. S. J. Sparks, T. C. Huang, and N. D. Watkins, 1978: The control of volcanic column heights by eruption energetics and dynamics. *J. Geophys. Res.,* **83** (83), 1829–1836.

Wohletz, K. H., M. F. Sheridan, and W. K. Brown, 1989: Particle size distributions and the sequential fragmentation/transport theory applied to volcanic ash. *J. Geophys. Res.,* **94** (B11), 15 703–15 721.

Wolfe, C. J., I. T. Bjarnason, J. C. VanDecar, and S. C. Solomon, 1997: Seismic structure of the Iceland plume. *Nature,* **385,** 245–247.

Zehner, C., Ed., 2010: Monitoring volcanic ash from space: ESA–EUMETSAT workshop on the 14 April to 23 May 2010 eruption at the Eyjafjoll volcano, south Iceland. ESA Publ. STM-280, 110 pp. [Available online at http://esamultimedia.esa.int/multimedia/publications/STM-280/.]

Zrnić, D. S., and A. Rhyzkov, 1996: Advantages of rain measurements using specific differential phase. *J. Atmos. Oceanic Technol.,* **13,** 454–464.